Cu(II) Pyrazolyl-benzimidazole Dinuclear Complexes with Remarkable Antioxidant Activity

Karim Chkirate,[a,*] Gamal Al Ati,[a] Khalid Karrouchi,[b] Saad Fettach,[c] Hind Chakchak,[d] Joel T. Mague,[e] Smaail Radi,[f] N. N. Adarsh,[g] My El Abbes Faouzi,[c] El Mokhtar Essassi,[a] and Yann Garcia[h,*]

[a] Laboratory of Heterocyclic Organic Chemistry URAC 21, Pharmacochemistry Competence Center, Av. Ibn Battouta, BP 1014, Faculty of Sciences, Mohammed V University in Rabat, Rabat 10010, Morocco.

[b] Laboratory of Analytical Chemistry and Bromatology, Faculty of Medicine and Pharmacy, Mohammed V University in Rabat, Morocco.

[c] Laboratory of Pharmacology and Toxicology, Biopharmaceutical and Toxicological Analysis Research Team, Faculty of Medicine and Pharmacy, Mohammed V University of Rabat, Morocco.

[d] Unités d'Appui Techniques À la Recherche Scientifique (UATRS), Centre National Pour la Recherche Scientifique et Technique (CNRST), Rabat, 10000, Morocco.

[e] Department of Chemistry, Tulane University, New Orleans, LA 70118, USA.

[f] LCAE, Département de Chimie, Faculté des Sciences, Université Mohamed Premier, BP 524, 60 000 Oujda, Morocco.

[g] Department of Chemistry & Biomolecular Science, Clarkson University, Potsdam, New York 13699, USA.

[h] Institute of Condensed Matter and Nanosciences, Molecular Chemistry, Materials and Catalysis (IMCN/MOST), Université catholique de Louvain, Place L. Pasteur 1, 1348 Louvain-la-Neuve, Belgium.

*Corresponding authors:

yann.garcia@uclouvain.be (Y. Garcia)

k.chkirate@um5r.ac.ma (K. Chkirate)

Abstract

Three dinuclear coordination complexes generated from 1-*n*-butyl-2-((5-methyl-1*H*-pyrazole-3-yl)methyl)-1*H*-benzimidazole (**L**), have been synthesized and characterized spectroscopically and structurally by single crystal X-ray diffraction analysis. Reaction with iron(II) chloride and then copper(II) nitrate led to a co-crystal containing 78% of $[Cu(NO_3)(\mu\text{-}Cl)(\mathbf{L}')]_2$ (**C₁**) and 22% of $[Cu(NO_3)(\mu\text{-}NO_3)(\mathbf{L}')]_2$ (**C₂**), where **L** was oxidized to a new ligand **L**'. A mechanism was provided. Reaction with copper chloride led to the dinuclear complex $[Cu(Cl)(\mu\text{-}Cl)(\mathbf{L})]_2$ (**C₃**). The presence of N–H···O and C–H···O intermolecular interactions in the crystal structure of **C₁** and **C₂**, and C–H···N and C–H···Cl hydrogen bonding in the crystal structure of **C₃** led to supramolecular structures which were confirmed by Hirshfeld surface analysis. The ligands and their complexes were tested for free radical scavenging activity and ferric reducing antioxidant power. The complex **C₁/C₂** shows remarkable antioxidant activities as compared to the ligand **L** and reference compounds.

Introduction

Reactive oxygen species (ROS) encompasses oxygen free radicals, such as superoxide anion radical ($O_2^{\cdot -}$) and hydroxyl radical ($^{\cdot}OH$), and nonradical oxidants, such as hydrogen peroxide (H_2O_2) and singlet oxygen ($^1O_2$). Thus, ROS are natural byproducts of cellular oxidative metabolism and play important roles in the modulation of cell survival, cell death, differentiation, cell signaling, and inflammation-related factor production. However, the excessive production of ROS gives rise to oxidative stress which is implicated in various pathologies such as diabetes, neurodegenerative diseases (Alzheimer's, Parkinson's), inflammatory diseases, cancers, aging, among others [1,2]. Cells use many antioxidant strategies to eliminate or minimize oxidative damage. Depending on the type, antioxidants can act by reducing ROS or trapping them to form a stable compound [3,4]. Antioxidant therapy has emerged as a tool to minimize biomolecular damage caused by ROS attack to vital constituents of living organisms and synthetic antioxidants have therefore received much attention from a pharmaceutical perspective [5]. Among the several types of antioxidants studied, a significant number of teams have focused on the role of metallodrugs as antioxidants [6-12].

Azole based compounds have attracted more attention in recent years due to their interesting biological and therapeutic properties [13-16]. Among azole-based compounds, in particular pyrazoles and benzimidazoles, are present in many clinical drugs, covering a wide range of biological properties [17-19]. Many transition metal complexes have been found to show various chemical, optical and magnetic properties [20, 21]. They have also been important in the development of new metal-based drugs [22] and, as a result, there has been a dramatic increase in the development and use of transition metal complexes as therapeutic drugs with promising pharmacological applications for the treatment of various human diseases [23]. Of particular interest are Cu(II) complexes since the pioneering work of Sorenson, which highlighted their great potential in biological use [24]. Copper(II) complexes have been widely studied since they have been found to be more active and desirable drugs with suppressed gastrointestinal toxicity as compared with the free and uncomplexed drug [25-28]. To date, a variety of *in vitro* biological activities of Cu(II) complexes are investigated including antimicrobial [29], anti-inflammatory [30], anticholinergic [31] and antiproliferative [32] properties. In particular, Cu(II) complexes tethered with heterocyclic moieties have received much interest as antioxidant agents [7, 9, 33-36].

Continuing research along this line [37-40], we have designed a new benzimidazole derivative functionalized with a pyrazole unit leading to **L**, namely 1-*n*-butyl-2-((5-methyl-1*H*-pyrazole-3-yl) methyl)-1*H*-benzimidazole (Scheme 1), by applying a recently conceived design approach [37]. A complexation reaction of **L** and Fe(II) chloride followed by addition of $Cu(NO_3)_2{\cdot}3H_2O$ led to an oxidation reaction involving the methylene group linking the benzimidazole and pyrazole moieties in **L** to form the ligand **L'** (Scheme 1). Reaction of **L** with only $CuCl_2{\cdot}2H_2O$ resulted in a complex with unaltered **L**. As complexing agents, we have used two different copper salts under different conditions in order to consider their influence on the course of the complexation reactions. Interestingly, three novel Cu(II) dinuclear complexes **C1–C3** including a co-crystal were obtained. Their crystal structure and their antioxidant activities are discussed, along with the ones of **L** and its precursor molecules **3** and **4** described in ref. [37].

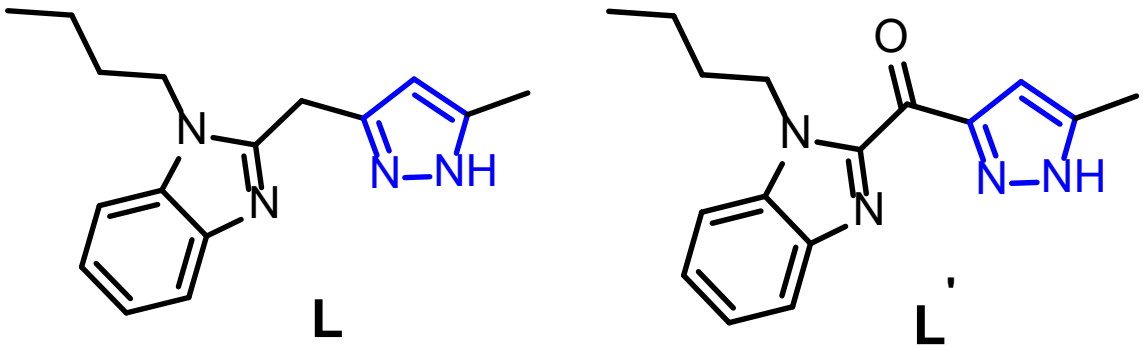

Scheme 1. Molecular structures of **L** and **L'**.

Results

Synthesis of L

Compounds **3**, **4** and the ligand **L** described here were synthesized according to a procedure from the literature [37] (Scheme 1).

Synthesis of coordination complexes C1/C2 and C3

The reaction of **L** in methanol with $FeCl_2{\cdot}4H_2O$ followed by addition of $Cu(NO_3)_2{\cdot}3H_2O$ dissolved in methanol with moderate heating gave single crystals of $[Cu(NO_3)(\mu\text{-}Cl)(\mathbf{L'})]_2$ (**C1**) and $[Cu(NO_3)(\mu\text{-}NO_3)(\mathbf{L'})]_2$ (**C2**) in the form of co-crystal of di(μ-chlorido)dinitrato(bis(1-*n*-butyl-2-(5-methyl-1*H*-pyrazole-3-carbonyl)-1*H*-1,3-benzodiazole)dicopper(II) and di(μ-nitrato)dinitratobis(1-*n*-butyl-2-(5-methyl-1*H*-pyrazole-3-carbonyl)-1*H*-1,3-benzodiazole)dicopper(II) which crystallizes in the triclinic system. It should be noted that the presence of $FeCl_2.4H_2O$ favors the oxidation of the methylene group linking the benzimidazole

and pyrazole rings [46,47] which is not observed when $CuCl_2 \cdot 2H_2O$ is used alone which results in crystals of formula $[Cu(Cl)(\mu\text{-}Cl)(\mathbf{L})]_2$ (**C3**) crystallizing in the monoclinic system. All complexes were characterized by single crystal X-ray diffraction.

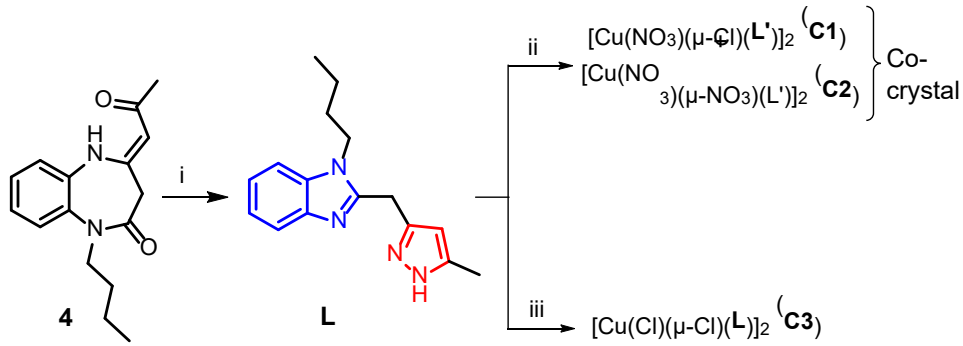

Scheme 2. Synthetic routes of **C1-C3**. i. $N_2H_4.H_2O$, EtOH; ii. $FeCl_2 \cdot 4H_2O/Cu(NO_3)_2 \cdot 3H_2O$, MeOH; iii. $CuCl_2 \cdot 2H_2O$, EtOH.

In the reaction condition (presence of $FeCl_2 \cdot 4H_2O$), ligand **L** undergoes an oxidation reaction by the oxygen in the air involving the methylene group linked to pyrazolic and benzimidazolic moieties. A plausible mechanism of this interesting oxidation reaction has been proposed on the basis of the oxidation of enaminic compound under the action of the oxygen in the air as shown in a previous works [39,40]. The ligand used can exist under two iminic and enaminic tautomeric forms **L** and $\mathbf{L_1}$. Thus, the enaminic tautomer $\mathbf{L_1}$ undergoes an oxidation reaction by the oxygen in the air to afford the spiro dioxetane [**A**] which undergoes a ring opening of the dioxetane moiety leading to the unstable intermediate [**B**] which aromatized after the loss of a water molecule to furnish the ligand **L'**. Then, the ligand **L'** undergoes a chelating reaction with Cu(II) nitrate (Scheme 3).

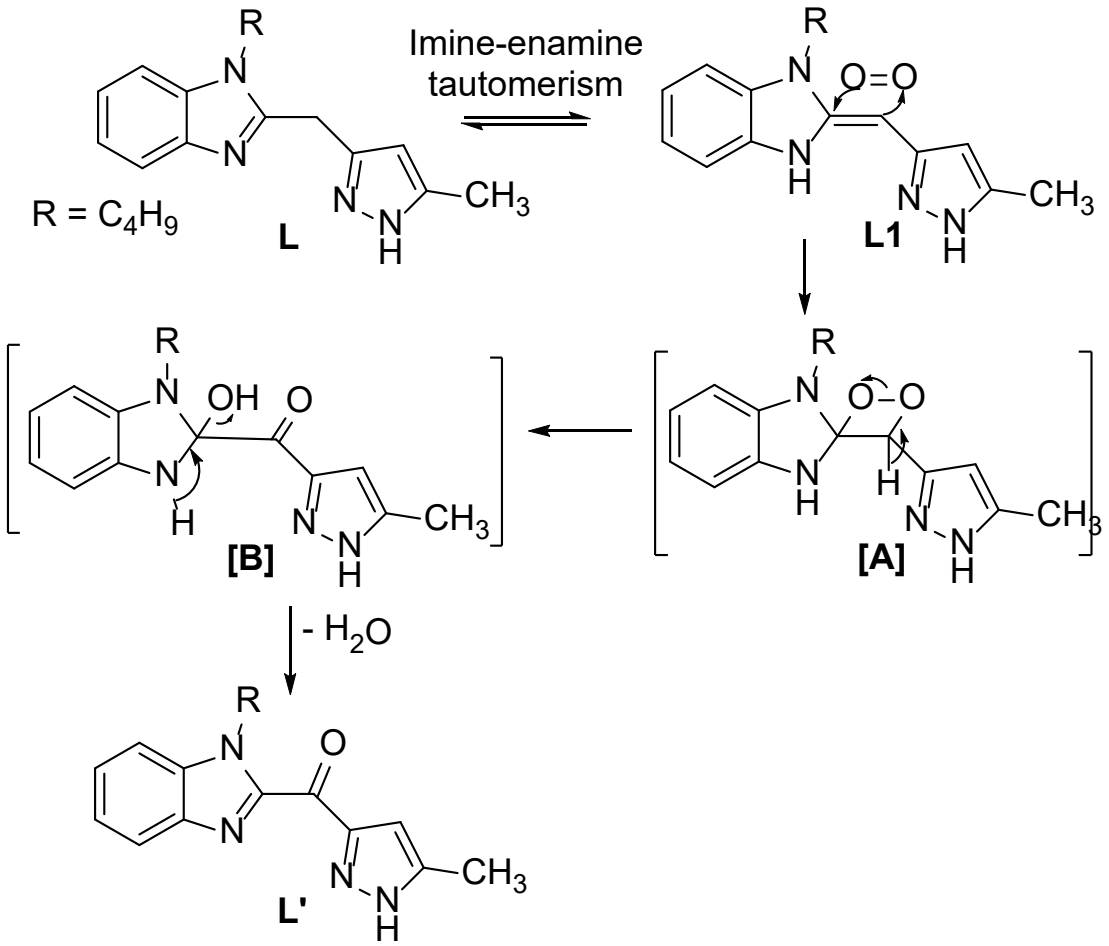

Scheme 3. Mechanism explaining the formation of Ligand **L'**.

Crystallography

Crystal structure of C_1/C_2

Light blue-green plate shaped crystals of $\mathbf{C_1/C_2}$ crystallized in the centrosymmetric triclinic space group *P-1*. A half-molecule of the coordination complex $\mathbf{C_1/C_2}$ is present in the asymmetric unit which consists of one fully occupied Cu(II), a full molecule of the ligand **L'**, one nitrate anion, a chloride anion (0.78 occupancy) and a second nitrate anion (0.22 occupancy) [all three are coordinated to the metal center]. The N atoms of the imidazole and pyrazole groups of the ligand are coordinated to the Cu(II) metal center which adopts a distorted square pyramidal geometry with basal anglesN3–Cu1–N1 = 86.58(9)°, O2–Cu1–N1 = 92.07(9)°, N3–Cu1–Cl1 = 91.00(7)°, O2–Cu1–Cl1 = 84.53(6)°, Cl1–Cu1–$Cl1^{i}$ = 162.51(8)° and O2–Cu1–N3 = 176.71(9)°. The basal positions of Cu(II) are occupied by the N1 and N3 atoms of the ligand **L'**, one nitrate anion (O2), and disordered nitrate or chloride (0.22:0.78 occupancy for nitrate:chloride). The apical position is occupied by the chloride or nitrate ligand

from the other half of the dimer so that the Cu–Cl distance is 2.3625(10) Å for the basal ligand and 2.6279(10) Å for the apical ligand while the respective Cu–O distances in the minor component are, respectively, 1.959(3) and 2.182(7) Å. The crystal structure of **C_1/C_2** is best described as a co-crystal of chlorido bridged (78%) and nitrato bridged (22%) Cu(II) dinuclear coordination complexes. The nitrato ligand showed asymmetric bidentate coordination to Cu(II) with Cu1–O2 and Cu1–O3 distances of 1.9661(19) and 2.818(3) Å, respectively in the major component but in the minor component, the terminal nitrate ligand shows a smaller degree of asymmetry in its coordination with Cu–O distances of 1.959(3) and 2.661(8) Å. An analysis of the coordination geometry of the major component with SHAPE [41] gave the smallest continuous shape measure (CShM) of 1.524 for the square pyramid with the next higher value being 2.539 for the "vacant octahedron" thus supporting the description given above as distorted square pyramidal (Fig. 1). The intramolecular N–H···O hydrogen bonding [H···O = 1.88 Å; N–H···O = 170°] involving the coordinated nitrate anion and pyrazole moiety helped to reinforce the coordination complex. The C=O group of the ligand is involved in a C–H···O intermolecular interaction [H···O = 2.59 Å; C–H···O = 160°] with the benzodiazole resulted in a one-dimensional (1D) chain as the primary supramolecular structure. The chains are assembled into a two-dimensional (2D) corrugated sheet structure parallel to (101) through C3–H3···O1 interactions (H···O = 2.52 Å; C–H···O = 168°). The layers are joined by offset π-stacking interactions between the 5-membered slippage = 1.51 Å) (Fig. 2). rings of the benzodiazole moieties (centroid···centroid = 3.7710(19) Å.

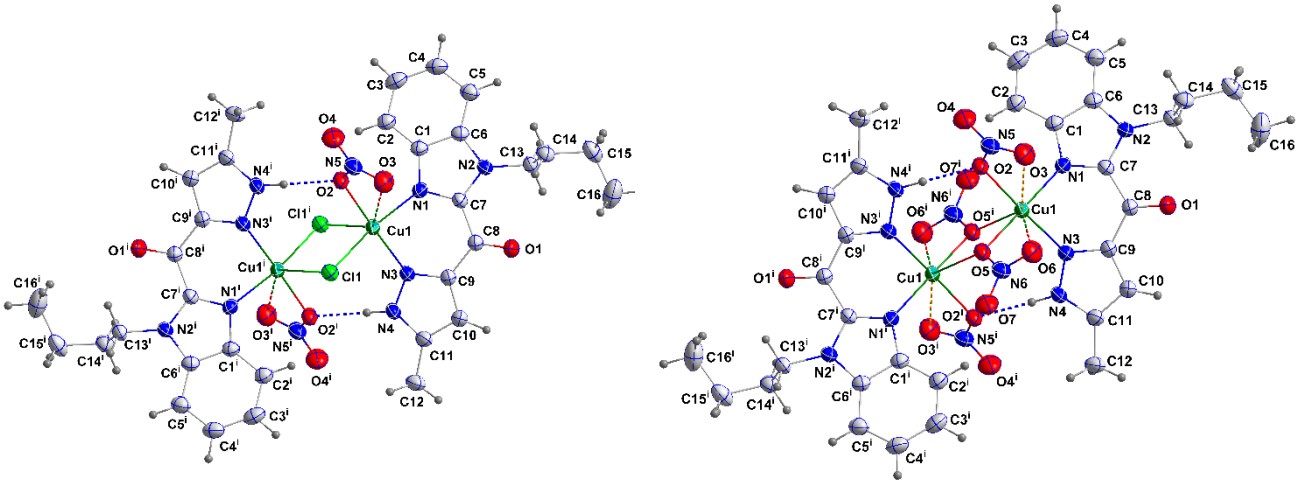

Figure 1. Perspective views of **C1** (left) and **C2** (right) with labelling schemes and 50% probability ellipsoids (symmetry code (i): -*x*+1, -*y*, -*z*+1).

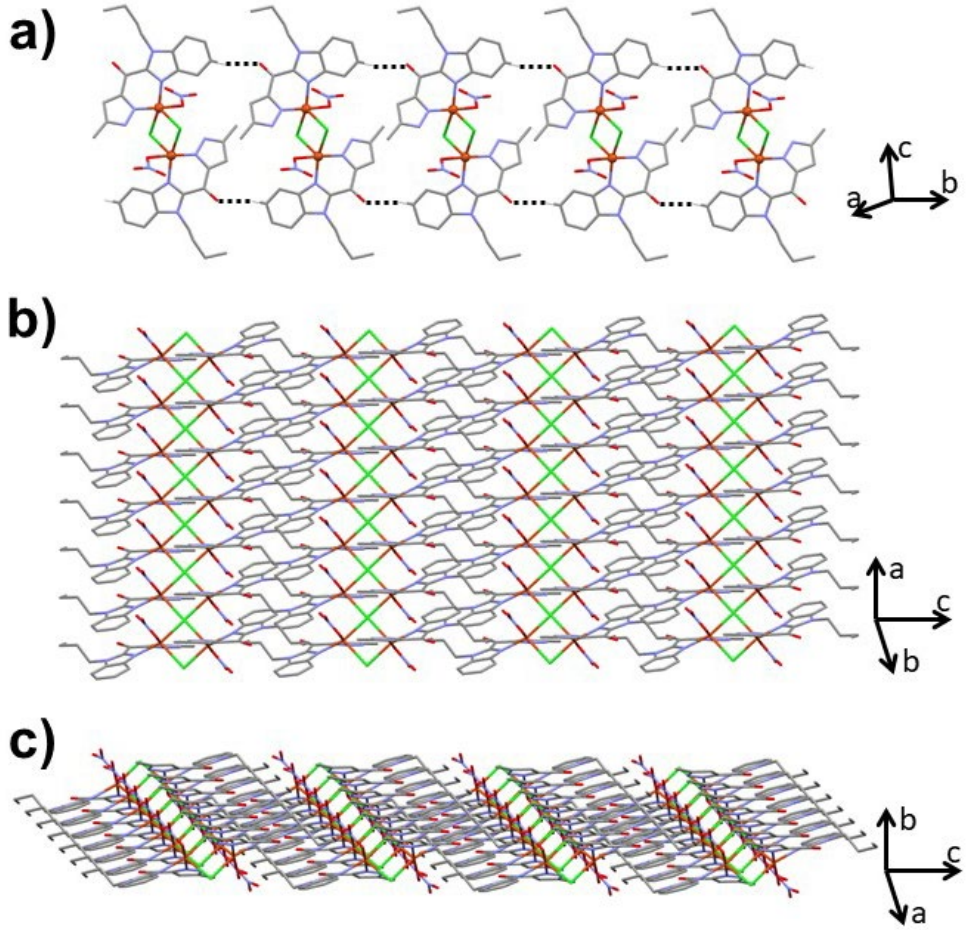

Figure 2. a) 1D chain hydrogen bonded synthon, b) and c) 2D corrugated sheet hydrogen bonded architecture of **C1**/**C2** in two different crystallographic axes.

Crystal structure of C3

The crystal of the coordination complex **C3** belongs to the monoclinic centrosymmetric space group $P2_1/c$. In the asymmetric unit, a half molecule of the coordination complex is present which consists of one Cu(II), one molecule of ligand and two chloride anions (both are coordinated to Cu(II)). The Cu(II) center adopts a distorted square pyramidal coordination geometry with basal angles N2–Cu1–Cl1 = 92.5(2)°, N3–Cu1–Cl2 = 89.4(2)°, N2–Cu1–N3 = 85.7(3)°, Cl1–Cu1–Cl2 = 90.98(9)°, N3–Cu1–Cl1 = 161.9(2)° and N2–Cu1–Cl2 = 173.9(2)°°.

The basal positions are occupied by the N2 and N3 atoms of the ligand and the bridging and terminal chloride anions and the apical position is occupied by the bridging chloride anion from the other half of the dinuclear complex (Fig. 3).

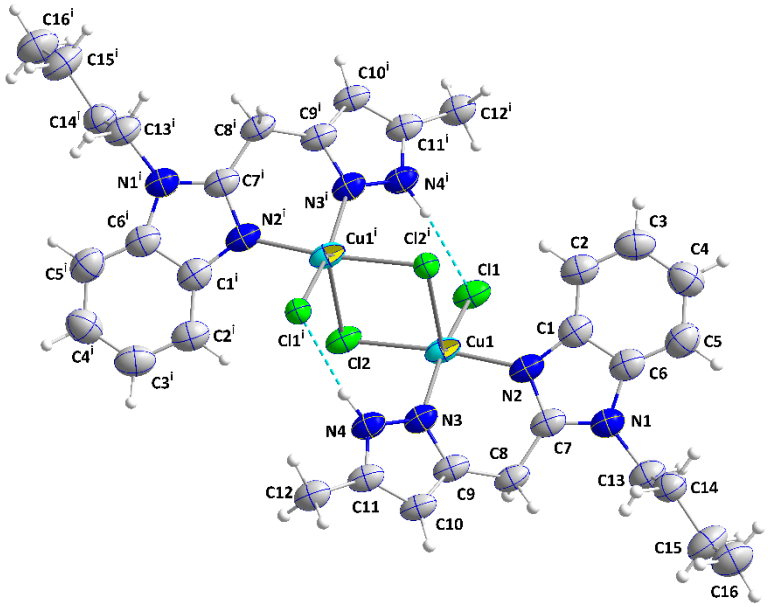

Figure 3. Perspective view of **C3** with labelling scheme and 50% probability ellipsoids. Intramolecular N–H···Cl hydrogen bonds are depicted by dashed lines (symmetry code: (i) -*x*+1, -*y*, -*z*+1).

Analysis of the coordination sphere gave a CShM value of 1.099 for the square pyramid and 1.925 for the vacant octahedron. The smaller CShM value obtained for **C3** as compared with **C1** indicates less distortion from the ideal coordination sphere for the former. **C3** is stabilized by N4–H4A···Cl1 hydrogen bonding [H4A···Cl1 = 2.38 Å, N4–H4A···Cl1 = 158°]. IN the crystal, 2D layers parallel to the *bc* plane are formed by C8–H8···N4 [H8···N4 = 3.482(12) Å; ∠C–H···N = 148°], C13–H13B···Cl2 and C14–H14A···Cl1 [H13B···Cl2 = 2.70 Å, C–H···C C13–H13B···Cl2 =168°; H14A···Cl1 = 2.77 Å, C14–H14A···Cl1 = 150°] hydrogen bonding (Fig. 4).

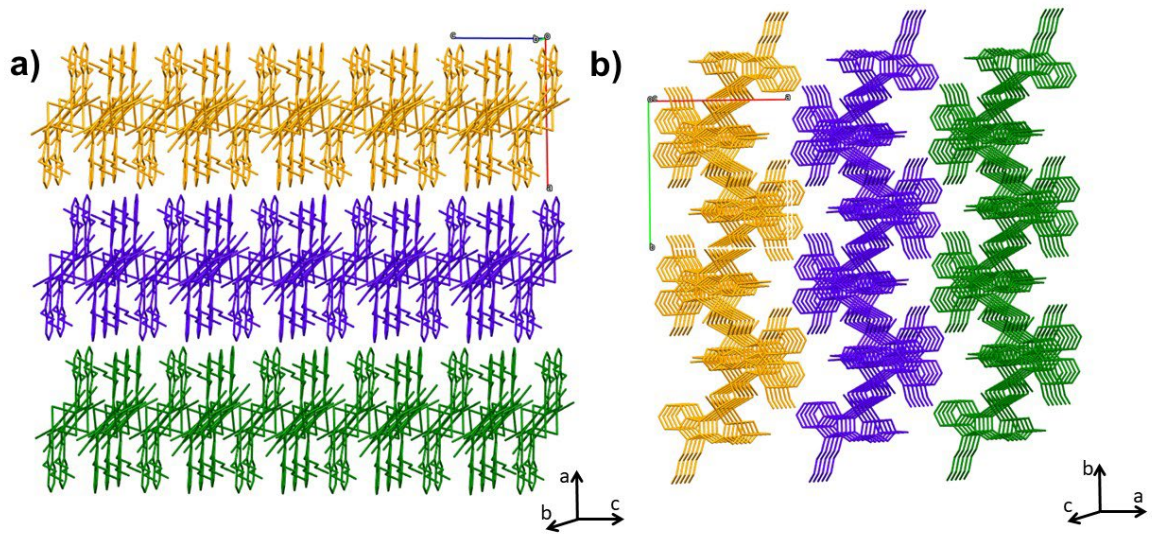

Figure 4. a) and b) off-set packing of 2D layered hydrogen bonded structure of **C3** in two distinct crystallographic axes.

Hirshfeld surface analysis

To further investigate the supramolecular interactions, present in **C1/C2** and **C3**, Hirshfeld surfaces were calculated with Crystal Explorer. Details of the procedures used and descriptions and interpretations of the plots obtained have been fully described [42].The existing hydrogen bonding present in the crystal structures of **C1/C2** (N–H···O) and C–H···O interactions, and **C3** (N–H···Cl, C-H···N, C–H···Cl) correspond well with their Hirshfeld surface data. Moreover, the red concave surface surrounded by receptors and the blue convex surface surrounding receptors on the Hirshfeld surfaces in the shape indices further support the presence of such hydrogen bonding (Fig. 5).

The 2D figure print plots (d_i vs d_e) show the contributions of the several supramolecular contacts in the complexes. The interatomic contacts to the Hirshfeld surface of **C1/C2** are C···H/H···C (14.4%), Cl···H/H···Cl (1.2%), H···H (30.6%), N···H/H···N (5.2%), O···H/H···O (34.3%), Cl···O (4.6%), C···O (1.5%) and C···C (3.7%). For **C3** are found Cl···H/H···Cl (19.4 %), N···H/H···N (6.2 %), C···H/H···C (18.1 %), H···H (52.1 %) and C···C (1%). The sharp spikes present in the 2D fingerprint plots revealed the presence of the strong N–H···O and C–H···O interactions in **C1/C2**, and N–H···Cl, C–H···N, C–H···Cl interactions in **C3**. The presence of

C···C in **C1/C2** (3.7%) and **C3** (1%) showed the contribution of C–H···π and/or π–π interactions (Fig. S1).

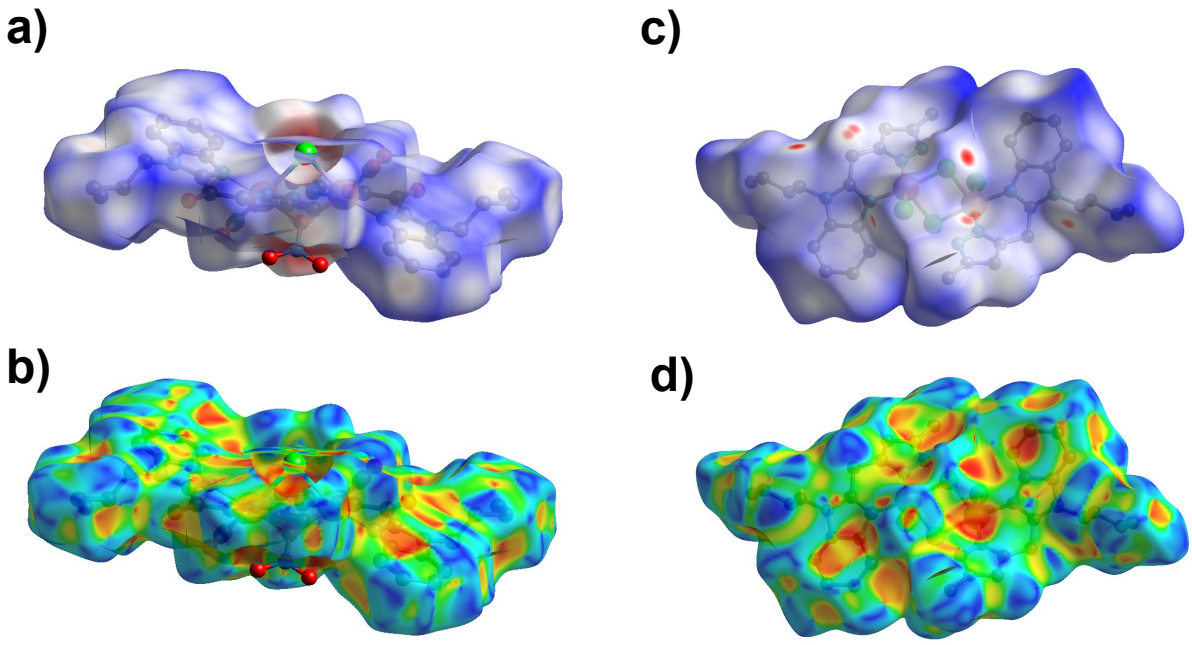

Figure 5. Hirshfeld surface mapped with the d_{norm} function for **C1/C2** (a) and **C3** (c). The interacting coordination complexes are shown in "ball and stick" model; Shape index of **C1/C2** (b) and **C2** (d), displaying hydrogen bonding and stacking interactions (shown red and blue triangles).

Antioxidant activity

Cu(II) coordination complexes have been widely explored for their potential antioxidant activities [7, 9, 12, 35, 38]. Still, significant improvements are of interest. In this context, we have investigated the antioxidant property of intermediates **3** and **4** (Scheme S2), **L**, **C1/C2**, and **C3**. The antioxidant activity of these compounds was systematically evaluated using three different assays namely DPPH, ABTS and ferric reducing antioxidant power (FRAP) (Table 1). Free radical scavenging is one of the best-known mechanisms by which antioxidants inhibit oxidation, and scavenging capacity is determined by measuring the decrease in absorption of 1,1-diphenyl-2-picrylhydrazyl acid (DPPH) and 2,2'-azino-bis(3-ethylbenzothiazoline-6-sulfonic acid) (ABTS) used as free radicals. Indeed, the DPPH assay is one of the most widely used methods to evaluate total antioxidant activity by determining free radical scavenging activity.

Also, the Ferric Reducing Antioxidant Power (FRAP) assay was used to determine the ability of the five compounds to reduce Fe^{3+} to Fe^{2+} with comparison of the results to those of the standards, trolox and dibutyl hydroxytoluene (BHT).

Table 1. Antioxidant activities of **3**, **4**, **L**, **C_1/C_2** and **C_3**.

Compound	DPPH IC_{50} (µM)	ABTS IC_{50} (µM)	FRAP µM EAA/ mM
3	313.35 ± 2.55	106.21± 1.62	400.4 ± 1.73
4	163.19 ± 1.05	149.62 ± 3.06	360.9 ± 1.91
L	152.02 ± 0.29	102.91± 0.89	540.4 ± 0.6
C_1-C_2	**92.12 ± 0.93**	**81.21 ± 1.07**	**1238.4 ± 0.43**
C_3	107.10 ± 1.18	113.20 ± 0.71	943.50 ± 2.95
BHT	99.06 ± 0.12	-	-
Trolox	-	77.71 ± 0.35	-

The DPPH test showed that **3**, **4** and **L** and the complexes **C_1/C_2** and **C_3** showed different degree of radical scavenging activity. Intermediates **3** and **4** and ligand **L** showed moderate activity compared to BHT, while **C_1/C_2** and to a minor extent **C_3** exhibited remarkable DPPH scavenging capacity with IC_{50} values of 92.12 µM and 107.10 µM, respectively, compared with that of standard BHT (99.06 µM) (Table 1).

For the ABTS assay, the antioxidant activity is based on the ability of the compounds to donate hydrogen or electrons by decolorizing the radical monocation of ABTS generated by oxidation with potassium persulfate. **3**, **4** and **L** were found to have good antioxidant activity compared to the reference Trolox (77.71 µM) whereas **C_1/C_2** presented the best antioxidant activity with a IC_{50} value of 81.21 µM (Table 1).

The reducing power of **L** and **C_1/C_2** and **C_3** was evaluated using the FRAP assay based on the ability of these compounds to reduce ferricyanide (Fe^{3+}) to ferrocyanide (Fe^{2+}). The results showed that the reducing power of **C_1/C_2** and **C_3** was higher compared to**L**, and even doubled for **C_1/C_2**. Results of this test are in good agreement with those of the DPPH and ABTS tests (Table 1).

Experimental

Syntheses

(Z)-4-(2-Oxopropylidene)-4,5-dihydro-1,5-benzodiazepin-2(3H)-one (**3**) (See Supporting Information).

(4Z)-1-Butyl-4-(2-oxopropylidene)-2,3,4,5-tetrahydro-1H-1,5-benzodiazepin-2-one (See Supporting Information).

1-n-Butyl-2-((5-methyl-1H-pyrazol-3-yl)methyl)-1H-benzimidazole (L). To a solution (2.6 mmol, 0.7 g) of 1-n-butyl-4-(2-oxopropylidene)-4,5-dihydro-1H-1,5-benzodiazepin-2(3H)-one in ethanol (15 mL) was slowly added hydrazine monohydrate (10.3 mmol, 0.5 mL). The reaction mixture was refluxed for 2 h. After cooling, the solution was concentrated to dryness. The residue was washed with absolute ethanol (10 mL) and a yellow solid was collected by filtration and dried in air. Yield: 98% (0.68 g); M.p. (°C): 115–117 °C (EtOH); IR (ATR, ν (cm^{-1})): 3190 (N–H), 2861–2965 (CH_3, CH_2), 1641 (C=N), 1615 (C=N); ^{1}H NMR (400 MHz, $CDCl_3$) δ ppm: 0.86 (t, 3H, C**H$_3$**–C_3H_6, *J* = 7.5 Hz); 1.30 (m, 2H, CH_2–C**H$_2$**–CH_3); 1.59 (m, 2H, CH_2–C**H$_2$**–CH_2); 2.18 (s, 3H, CH_3–pyraz.); 4.05 (m, 2H, N–CH_2); 4.25 (s, 2H, benzim. –$CH_{2pyraz.}$); 5.87 (s, 1H, $CH_{pyraz.}$); 7.20–7.65 (m, 4H, H_{ar}); 9.57 (s, 1H, NH); ^{13}C NMR (400 MHz, $CDCl_3$) δ ppm: 11.57 (CH_3–C_3H_6), 13.70 (CH_3-pyraz.), 20.12 (CH_2–CH_2–CH_3), 26.95 (benzim. –CH_2–pyraz.), 31.68 (CH_2–CH_2–CH_2), 43.75 (N–CH_2), 103.94 ($CH_{pyraz.}$), 119.18 (CH_{ar}), 122.27 (CH_{ar}), 135.15 ($C_{q\ ar}$), 142.26 ($C_{q\ ar}$), 142.67 (C_q=$N_{pyraz.}$), 151.98 (N–C_q=N); ESI-MS (MeOH): *m/z* = 269.7 $[M+H]^+$, 291.0 $[M+Na]^+$. UV/Vis (DMSO): λ_{max} = 280, 305, 345 nm.

[Cu(NO$_3$)(μ-Cl)(L')]$_2$ (C$_1$) and [Cu(NO$_3$)(μ-NO$_3$)(L')]$_2$ (C$_2$). $FeCl_2{\cdot}4H_2O$ (1 mmol, 198 mg) was dissolved in methanol (15 mL) and added to a solution of **L** (1 mmol, 269 mg) in methanol (15 mL). The mixture was refluxed for 15 min. After cooling, the precipitate was isolated and then solubilized in methanol (15 mL) and added to a solution of $Cu(NO_3)_2{\cdot}3H_2O$ (1 mmol; 241 mg) in methanol (15 mL). The mixture was refluxed for 15 min. After cooling, the precipitate was isolated and recrystallized from a mixture of ethyl acetate and ethanol (1:1). After 24 h of slow evaporation at room temperature, light blue-green plate-shaped single crystals were obtained and isolated. Yield: 64% (172 mg); FT-IR (ATR, (cm^{-1})): 3182-2863 (CH), 1575 (C=O); 1478 (C=N); 1448, 1414 (C=C), 524 (Cu-O), 434 (Cu-N); UV/Vis (DMSO): λ_{max} = 274, 281 nm; ESI-HRMS: *m/z* = 894.4137 $[M + H]^+$ for $C_{32}H_{36}Cu_2Cl_2N_{10}O_8$ in MeOH.

[Cu(Cl)(μ-Cl)(L)]$_2$ (C_3). $CuCl_2 \cdot 2H_2O$ (1 mmol, 170 mg) was dissolved in ethanol (15 mL) and added to a solution of L_1 (1 mmol, 269 mg) in ethanol (15 mL). The reaction mixture was heated slightly and the resulting light green solution was left at room temperature. Single crystals in the shape of blue plates were obtained through slow evaporation of the reaction mixture for 24 h. Yield: 40% (107 mg); FT-IR (ATR, (cm^{-1})): 3187 (NH), 3132-2865 (CH), 1613 (C=N); 1570, 1489, 1458 (C=C), 412 (Cu-Cl), 426 (Cu-N); UV/Vis (DMSO): λ_{max} = 273, 280 nm; ESI-HRMS: *m*/*z* = 769.0976 $[M\text{-}Cl + H]^+$ for $C_{32}H_{40}Cl_4Cu_2N_8$ in MeOH.

Characterization methods

Melting points were measured using a Buchi B-545 digital capillary melting point apparatus and are uncorrected. Reactions were checked with TLC using aluminum sheets coated with silica gel 60 F254 from Merck. IR spectra were recorded on a PerkinElmer VERTEX 70 FT-IR spectrometer covering the range 400–4000 cm^{-1}. ^1H and ^{13}C NMR spectra were recorded in DMSO-d_6 and $CDCl_3$ on a Bruker spectrometer (400 MHz). Chemical shifts are expressed in ppm by using tetramethylsilane (TMS) as an internal reference. Mass spectra were collected in MeOH using an API 3200 LC/MS/MS system, equipped with an ESI source. UV-vis spectra were recorded on an Analytik Jena, Specord 210 plus spectrophotometer over the range 200-800 nm.

X-ray crystallography

Single crystal X-ray data for **C_1**/**C_2** and **C_3** were collected at 150 K using Cu Kα (λ = 1.54178 Å) radiation on a Bruker D8 VENTURE PHOTON 100 CMOS diffractometer. Data collection was performed using the *APEX3* diffractometer control software [43]. Conversion of the raw intensity data to F^2 values was accomplished with *SAINT* [43] which also performed a global refinement of unit cell parameters. Empirical corrections for absorption and merging of equivalent reflections employed *SADABS* [44] for **C_1**/**C_2** and *TWINABS* [45] for **C_3**. The structures were solved by dual space methods (*SHELXT* [46]) and refined by full-matrix, least-squares procedures (*SHELXL* [47]). The nonhydrogen atoms were treated anisotropically while hydrogen atoms attached to carbon were included as riding contributions with isotropic displacement parameters tied to those of the attached atoms. Those attached to nitrogen were located on a difference Fourier map, their coordinates adjusted to give N–H 0.91 Å and were included as riding contributions as for the others. For **C_1**/**C_2**, it became evident that one of the bridging sites was partially occupied by a nitrate ion. Because of the crystallographically-

imposed centrosymmetry, the crystal was best considered to be a co-crystal of the di(μ-nitrato) complex and the di(μ-chlorido) complex. Attempts to refine the occupancy factors for the overlapping bridging chlorido and nitrato ligands were not particularly successful even treating the nitrate as a rigid group so approximate values were obtained by making the displacement parameters for the fully and partially occupied nitrato sites comparable. This gave a 78:22 mixture of the di(μ-chlorido) complex and the di(μ-nitrato) complex. For **C3**, analysis of 710 reflections having I/σ(I) > 12 and chosen from the full data set with *CELL_NOW* [48] showed the crystal to belong to the monoclinic system and to be twinned by a 180° rotation about the *b* axis. The raw data were processed using the multi-component version of *SAINT* under control of the two-component orientation file generated by *CELL_NOW*. The final model was refined as a 2-component twin. CCDC 2232892 and 2232893 contain the supplementary crystallographic data for this paper.

Hirshfeld surface analysis

The Hirshfeld surfaces of the coordination complexes and the corresponding 2D fingerprint plots were obtained by using the software package CRYSTAL EXPLORER 17.5.43 and d-plot is used to measure the distances to the surface from nuclei outside (d_e) and inside (d_i) the Hirshfeld surface. The d_{norm} surface is plotted over a fixed colour scale of -0.25 a.u. (red) to -0.95 a.u. (blue). The shape index plot is mapped in the colour range -1.0 a.u. (concave) to 1.0 a.u. (convex) and the curvedness plot in the range of -4.0 a.u. (flat) to -0.4 (singular). The 2D fingerprint plots were displayed in the 0.5–2.8 Å range, including reciprocal contacts.

The normalized contact between the molecules is denotated as d_{norm}, which can be easily calculated by using eq. (1):

$$d_{norm} = \frac{d_i - r_i^{vdW}}{r_i^{vdW}} + \frac{d_e - r_e^{vdW}}{r_e^{vdW}} \quad (1)$$

In eq. (1), d_i and d_e belong to the distance between the Hirshfeld surface and the closest nucleus inside the surface and nearby nucleus outside the surface, respectively. In addition, r_i^{vdW} and r_e^{vdW} are the van der Waals radii of the atoms. The normalized short contact d_{norm} is plotted between d_i and d_e.

Antioxidant activity

DPPH radical scavenging activity

The radical-scavenging activity of **3, 4**, **L**, **C_1/C_2** and **C_3** were evaluated vs. the stable 1,1-diphenyl-2-picrylhydrazyl acid (DPPH) radical, according to the method described previously [39]. In this procedure, 2 mL of a 4 % solution of DPPH in methanol (w/v) was mixed with 500 µL of sample solutions at different concentrations (15-1500 µM). The scavenging capacity was determined spectrophotometrically after 30 min of incubation by monitoring the decrease of the absorbance at λ = 517 nm. Lower absorbance of the reaction mixture indicates higher free radical scavenging activity. Ascorbic acid was used as standard. The percent DPPH scavenging effect was calculated using the following equation:

$$\% \text{ of scavenging} = [(A_c - A_t)/A_c] \times 100$$

where A_c is the absorbance of the control sample (DPPH solution without test sample) and A_t is the absorbance of the test sample (DPPH solution + test compound). Tests were performed in triplicate, and the results averaged.

ABTS radical scavenging activity

The ABTS (2,2'-azino-bis (3-ethylbenzothiazoline-6 sulfonic acid) free radical-scavenging activity of **3, 4**, **L**, **C_1/C_2** and **C_3** was estimated using the method described previously [39]. The blue-green ABTS radical cation was produced by reaction between 7mM ABTS and 70mM potassium persulfate in water. The mixture was stored at room temperature in the darkness for 16h prior use. The ABTS solution was then diluted with 80% MeOH to obtain an absorbance of 0.700 ± 0.005 at λ = 734 nm. One hundred microliters of sample solutions at different concentrations (125-2000 µM) were added to 2 mL of ABTS solution and the absorbance was recorded at λ = 734 nm after 1 min incubation at room temperature. This was compared to the blank where 200 µL of the methanol was added to 2 mL of ABTS solution. A standard curve was obtained by using 3,4-dihydro-6-hydroxy-2,5,7,8-tétraméthyl-2H-1-benzopyran-2-carboxylic acid (Trolox) as a reference solution at various concentrations. The scavenging activities of different concentrations of synthesized compounds against ABTS radical were also measured to calculate the IC_{50}, and the procedure was similar to the DPPH scavenging method described above. The test was carried out in triplicate and IC_{50} values were reported as means ± SD.

$$\% \text{ Inhibition} = (A_c - A_t/A_c) / 100$$

Where A_c is the absorbance of the control, and A_t is the absorbance in the presence of the samples or reference. The control did not contain compound or standard.

Ferric Reducing/Antioxidant Power (FRAP) Assay

The ferric-reducing capacity of the ligands and complexes was investigated by using the potassium ferricyanide-ferric chloride method [39]. Briefly, the sample (1 mL) at 1 mM was mixed with 2.5mL of phosphate buffer (0.2M, pH = 6.6) and 2.5 mL of 1% $K_3[Fe(CN)_6]$. The mixture was then incubated at 50 °C for 20 min to reduce ferricyanide into ferrocyanide. A portion (2.5 mL) of trichloroacetic acid (10 %) was added to the mixture which was then centrifuged at 3000 rpm for 10 min. Finally, 2.5mL of the supernatant was mixed with distilled water (2.5 mL) and 0.5 mL of a $FeCl_3$ solution (0.1%, w/v), and the absorbance was measured at λ = 700 nm. Increased absorbance values indicate a higher reducing power. The results were expressed as ascorbic acid equivalent per gram of product dry weight (µM AAE/mM comp).

Conclusions

In summary, three new dinuclear Cu(II) complexes with 1-*n*-butyl-2-((5-methyl-1*H*-pyrazole-3-yl)methyl)-1*H*-benzimidazole (**L**) were synthesized and characterized. Reaction of **L** with Cu(II) nitrate in the presence of Fe(II) chloride led to a co-crystal of formula $[Cu(NO_3)(\mu\text{-}Cl)(\mathbf{L'})]_2$ (**C₁**) and $[Cu(NO_3)(\mu\text{-}NO_3)(\mathbf{L'})]_2$ (**C₂**) where **L** was oxidized to a new ligand **L'**. A dinuclear complex $[Cu(Cl)(\mu\text{-}Cl)(\mathbf{L})]_2$ (**C₃**) was formed too by the reaction of **L** with Cu(II) chloride alone. The crystal structure of **C₁/C₂** is best described as a co-crystal of chloro bridged (78%) and nitrato bridged (22%) Cu(II) dinuclear coordination complexes. The hydrogen bonding present in the crystal structures of the complexes **C₁/C₂** (N–H···O, C–H···O) and **C₃** (N–H···Cl, C-H···N, C–H···Cl) as well as and π···π stacking in the former led to supramolecular structures which correspond well with their Hirshfeld surface analyses. Complex **C₁/C₂** exhibited a strong antioxidant activity compared to reference molecules (BHT and trolox). Such dinuclear complex, by their short Cu···Cu distances (below 3.5 Å), are anticipated to present too interesting cooperative magnetic properties with a long-range order [49].

Conflicts of interest

There are no conflicts to declare.

Acknowledgements

This work was supported by a bilateral WBI action with Morocco (project 4.3 Program 2018-2022), the Fonds De La Recherche Scientifique – FNRS (PDR T.0102.15, CDR J.0064.23) and the COST action ACRYRED 21149.

Keywords

Antioxidant activity, benzimidazole, copper, dinuclear complexes, Hirshfeld surface analysis

Notes and references

[1] P. Poprac, K. Jomova, M. Simunkova, V. Kollar, C. J. Rhodes, M. Valko, *Trends in Pharmacol. Sci.*, **2017**, 38, 592-607.

[2] J. D. Hayes, A. T. Dinkova-Kostova, K. D. Tew, *Cancer cell.*, **2020**, 38, 167-197.

[3] W. Wang, and P. M. Kang, *Antioxidants*, **2020**, 9, 1292.

[4] R. Vona, N. M. Sposi, L. Mattia, L. Gambardella, E. Straface, D. Pietraforte, *Antioxidants*, **2021**, 10, 296.

[5] H. O. Ammar, R. N. Shamma, R. S. Elbatanony, B. Khater, *Sci. Pharm.*, **2020**, 88, 5.

[6] A. Haber, Z. Gross, *Chem. Commun.*, **2015**, 51, 5812-5827.

[7] J. F. Guerreiro, M. A. G. Gomes, F. Pagliari, J. Jansen, M. G. Marafioti, C. Nistico, and J. Seco, *RSC Advances*, **2020**, 10, 12699-12710.

[8] I. Yousuf, M. Bashir, F. Arjmand, S. Tabassum, *Coord. Chem. Rev.*, **2021**, 445, 214104.

[9] G. Psomas, Copper(II) and zinc(II) coordination compounds of non-steroidal anti-inflammatory drugs: Structural features and antioxidant activity. *Coord. Chem. Rev.*, **2020**, 412, 213259.

[10] S. Veeralakshmi, S. Nehru, G. Sabapathi, S. Arunachalam, P. Venuvanalingam, P. Kumar, V. Ravikumar, *RSC Advances*, **2015**, 5, 31746-31758.

[11] E. Halevas, B. Mavroidi, M. Pelecanou, A. G. Hatzidimitriou, *Inorg. Chim. Acta*, **2021**, 523, 120407.

[12] I. Mantasha, M. Shahid, M. Ahmad, R. Arif, S. Tasneem, F. Sama, I. A. Ansari, *New J. Chem.*, **2019**, 43, 622-633.

[13] M. Sharma, P. Prasher, *Med. Chem.*, **2020**, 11, 184-211.

[14] K. Karrouchi, S. Radi, Y. Ramli, J. Taoufik, Y. Mabkhot, F. Al-aizari, M. Ansar. A Review. *Molecules*, **2018**, 23, 134.

[15] I. J. de Esch, D. A. Erlanson, W. Jahnke, C. N. Johnson, L. Walsh, *J. Med. Chem.*, **2021**, 65, 84-99.

[16] Y. Garcia, *Adv. Inorg. Chem*., **2020**, 76, 121-153.

[17] N. Kerru, L. Gummidi, S. Maddila, K. K. Gangu, S. B. A. Jonnalagadda, *Molecules*, **2020**, 25, 1909.

[18] R. S. Keri, A. Hiremathad, S. Budagumpi, B. M. Nagaraja, *Chem. Biol. Drug. Des.*, **2015**, 86, 19-65.

[19] M. J. Akhtar, M. S. Yar, V. K. Sharma, A. A. Khan, Z. Ali, M. D. Haider, A. Pathak, *Curr. Med. Chem.*, **2020**, 27, 5970-6014.

[20] A. Steinbrueck, J. Karges, *ChemBioChem*, **2023**, e202300079.

[21] O. Desiatkina, G. Boubaker, N. Anghel, Y. Amdouni, A. Hemphill, J. Furrer, E. Păunescu, *ChemBioChem*, **2022,** 23, e202200536.

[22] P. Jia, R. Ouyang, P. Cao, X. Tong, X. Zhou, T., Lei, and S. Zhou, *J. Coord. Chem.*, **2017**, *70*, 2175-2201.

[23] K. O. Marichev, S. A. Patil, S. A. Patil, H. M. Heras Martinez, A. Bugarin, *Expert Opin. Ther. Pat.* **2022**, *32*, 47-61.

[24] J. R. Sorenson, Springer Science & Business Media, 2012.

[25] A. Hussain, M. F. AlAjmi, M. T. Rehman, S. Amir, F. M. Husain, A. Alsalme, R. A. Khan, *Sci. Rep.*, **2019**, 9, 5237.

[26] A. Ahmedova, B. Todorov, N. Burdzhiev, C. Goze, *Eur. J. Med. Chem.*, **2018**, 157, 1406-1425.

[27] Y. Li, *IUBMB life*, **2020**, 72, 1900-1908.

[28] S. Baldari, G. Di Rocco, G Toietta, Int. J. Mol. Sci, **2020**, 21, 1069.

[29] N. Revathi, M. Sankarganesh, J. Dhaveethu Raja, S. Johnson Raja, S. Gurusamy, R. Nandini Asha, T. C. Jeyakumar, *J. Biomol. Struct. Dyn.***2023**, 1-15.

[30] M. Manjunatha, V. H. Naik, A. D. Kulkarni, S. A. Patil, *J. Coord. Chem.*, **2011**, *64*, 4264-4275.

[31] A. Barmpa, A. G. Hatzidimitriou, G. Psomas, *J. Inorg. Biochem.*, **2021**, *217*, 111357.

[32] J. P. Rada, J. Forté, G. Gontard, V. Corce, M. Salmain, N. A. Rey, *ChemBioChem*, **2020**, *21*, 2474-2486.

[33] G. García-Díez, R. Ramis, N. Mora-Diez, *ACS Omega*, **2020**, 5, 14502-14512.

[34] A. Tăbăcaru, R. A. Khan, G. Lupidi, C. Pettinari, *Molecules*, **2020**, 25, 5298.

[35] X. Tang, Y. Qu, C. Wang, Y. Wu, K. Zhao, H. Wu, *J. Chin. Chem. Soc.,* **2020***,* 67, 585-591.

[36] H. Wu, Y. Zhang, H. Chen, J. Liu, L. Xiu, J. Huang, *Inter. J. Biolog. Macromol*., **2023**, 231, 123200.

[37] K. Chkirate, K. Karrouchi, N. Dege, N. K. Sebbar, A. Ejjoummany, S. Radi, N. N. Adarsh, A. Talbaoui, M. Ferbinteanu, E. M. Essassi, Y. Garcia. *New J. Chem*., **2020**, 44, 2210-2221.

[38] K. Chkirate, S. Fettach, K. Karrouchi, N. K. Sebbar, E. M. Essassi, J. T. Mague, Y. Garcia, *J. Inorg. Biochem.*, **2019**, 191, 21-28.

[39] K. Chkirate, S. Fettach, M. El Hafi, K. Karrouchi, B. Elotmani, J. T. Mague, S. Radi, M. E. A. Faouzi, N. N. Adarsh, E. M. Essassi, Y. Garcia, *J. Inorg. Biochem.,* **2020**, 208, 111092.

[40] K. Chkirate, K. Karrouchi, H. Chakchak, J. T. Mague, S. Radi, N. N. Adarsh, W. Li, A. Talbaoui, E. M. Essassi, Y. Garcia, *RSC Advances*, **2022**, 12, 5324-5339.

[41] M. Lunell, D. Casanova, J. Cirera, P. Alemany, S. Alvarez, SHAPE, Department de Quimica Fisica, Department de Quimica Inorgànica and Institut de Quimica Teòrica i Computacional-Universitat de Barcelona, **2013**.

[42] S. L. Tan, M. M. Jotani E. R. T. Tiekink, *Acta Cryst.,* **2019**, E75, 308-318.

[43] APEX3 and SAINT, Bruker AXS, Madison, WI, USA, **2019**.

[44] L. Krause, R. Herbst-Irmer, G.M. Sheldrick, D. J. Stalke, *Appl. Cryst.,* **2015**, 48, 3-10.

[45] G. M. Sheldrick, *TWINABS*, University of Göttingen, Göttingen, Germany, **2009**.

[46] G. M. Sheldrick, *Acta Cryst*., **2015**, A71, 3-8.

[47] G. M. Sheldrick, *Acta Cryst.,* **2015**, C71, 3-8.

[48] G. M. Sheldrick, *CELL_NOW*, University of Göttingen, Göttingen, Germany, **2008**.

[49] Y. Garcia, P. J. van Koningsbruggen, G. Bravic, D. Chasseau, O. Kahn, *Eur. J. Inorg. Chem*., **2003**, 356-362.

Table of Contents (ToC) entry

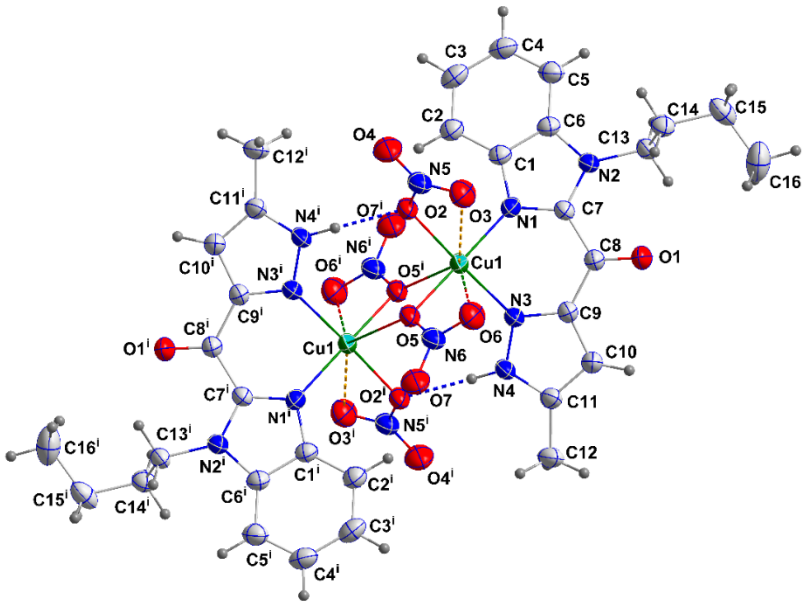

The novel dinuclear Cu(II) complex $[Cu(NO_3)(\mu\text{-}NO_3)(\mathbf{L'})]_2$, containing an oxidized ligand, shows remarkable antioxidant properties as compared to the original ligand and reference compounds. A mechanism was provided.